Published in final edited form as:
Eur J Nucl Med Mol Imaging. 2013 May ; 40(5): 759–767. doi:10.1007/s00259-012-2334-2.

PET Imaging of CD105/Endoglin Expression with a $^{61/64}$Cu-Labeled Fab Antibody Fragment

Yin Zhang[1,#], **Hao Hong**[2,#], **Hakan Orbay**[2], **Hector F. Valdovinos**[1], **Tapas R. Nayak**[2], **Charles P. Theuer**[3], **Todd E. Barnhart**[1], and **Weibo Cai**[1,2,4,*]

[1]Department of Medical Physics, University of Wisconsin - Madison, WI, USA

[2]Department of Radiology, University of Wisconsin - Madison, WI, USA

[3]TRACON Pharmaceuticals, Inc., San Diego, CA, USA

[4]University of Wisconsin Carbone Cancer Center, Madison, WI, USA

Abstract

Purpose—The goal of this study was to generate and characterize the Fab fragment of TRC105, a monoclonal antibody that binds with high affinity to human and murine CD105 (i.e. endoglin), and investigate its potential for positron emission tomography (PET) imaging of tumor angiogenesis in a small animal model after $^{61/64}$Cu-labeling.

Methods—TRC105-Fab was generated by enzymatic papain digestion. The integrity and CD105 binding affinity of TRC105-Fab was evaluated before NOTA (i.e., 1,4,7-triazacyclononane-1,4,7-triacetic acid) conjugation and $^{61/64}$Cu-labeling. Serial *PET* imaging and biodistribution studies were carried out in the syngeneic 4T1 murine breast cancer model to quantify tumor targeting efficacy and normal organ distribution of $^{61/64}$Cu-NOTA-TRC105-Fab. Blocking studies with unlabeled TRC105 were performed to confirm CD105 specificity of the tracer in vivo. Immunofluorescence staining was also conducted to correlate tracer uptake in the tumor and normal tissues with CD105 expression.

Results—TRC105-Fab was produced with high purity through papain digestion of TRC105, as confirmed by SDS-PAGE, HPLC analysis, and mass spectrometry. $^{61/64}$Cu-labeling of NOTA-TRC105-Fab was achieved with ~50% yield (specific activity: ~44 GBq/μmol). PET imaging revealed rapid uptake of ^{64}Cu-NOTA-TRC105-Fab in the 4T1 tumor (3.6 ± 0.4, 4.2 ± 0.5, 4.9 ± 0.3, 4.4 ± 0.7, and 4.6 ± 0.8 %ID/g at 0.5, 2, 5, 16, and 24 h post-injection respectively; n = 4). Since tumor uptake peaked soon after tracer injection, ^{61}Cu-labeled TRC105-Fab was also able to provide tumor contrast at 3 and 8 h post-injection. CD105 specificity of the tracer was confirmed with blocking studies and histological examination.

Conclusion—Herein we report PET imaging of CD105 expression with $^{61/64}$Cu-NOTA-TRC105-Fab, which exhibited prominent and target specific uptake in the 4T1 tumor. The use of a Fab fragment led to much faster tumor uptake (which peaked at a few hours after tracer injection) compared to radiolabeled intact antibody, which may be translated into same day immunoPET imaging for clinical investigation.

Requests for reprints: Weibo Cai, PhD, Departments of Radiology and Medical Physics, University of Wisconsin - Madison, Room 7137, 1111 Highland Avenue, Madison, WI 53705-2275, USA, wcai@uwhealth.org; Phone: 608-262-1749; Fax: 608- 265-0614.
[#]These authors contributed equally to this work

Conflicts of interest C.P.T. is an employee of TRACON Pharmaceuticals, Inc. The other authors declare no conflicts of interest.

Keywords

Positron emission tomography (PET); Tumor angiogenesis; Antibody fragment; Fab; CD105 (endoglin); ^{61}Cu; ^{64}Cu

Introduction

The growth and metastasis of most solid tumors depends on angiogenesis, without which they cannot grow beyond a few millimeters in size [1]. During the last decade, a myriad of studies have been published on tumor angiogenesis (especially with the use of molecular imaging techniques), making it an extremely dynamic research area [2–4]. The most widely studied angiogenesis-related targets include integrin $\alpha_v\beta_3$, vascular endothelial growth factor receptors (VEGFRs), and CD105 (i.e. endoglin) [3–10]. Several tracers targeting these receptors are already under clinical investigation [3, 7, 9].

Primarily overexpressed on proliferating endothelial cells, CD105 has recently emerged as a promising candidate for tumor vascular targeting [8, 11, 12]. CD105 immunohistochemistry is now the accepted standard approach for identifying actively proliferating tumor vessels. High CD105 microvessel density (MVD) correlates with poor prognosis in multiple tumor types, including breast cancer [11].

To date, positron emission tomography (PET) imaging of CD105 has not been investigated in the clinic. Future translation of the optimized PET tracer(s) for CD105 imaging (i.e. non-invasive full body MVD measurement) can play multiple roles in improving the management of cancer patients. We recently reported the first PET imaging of CD105 expression in a mouse model of breast cancer using a ^{64}Cu-labeled chimeric monoclonal antibody TRC105, which has high avidity for both human and murine CD105 [13]. A multicenter Phase 1 first-in-human dose-escalation trial of TRC105 has been completed and multiple Phase 2 trials are underway in a number of solid tumor types [14].

One major limitation of imaging/diagnostic agents based on intact antibodies is the prolonged circulation half-life [15]. Typically, tumor uptake does not reach the peak until a few days after tracer injection. This has motivated the development of antibody fragment-based imaging probes that exhibit good targeting efficacy and rapid blood clearance to allow for the potential same day imaging in the clinic [16–25]. IgG antibodies are composed of Fc and Fab fragments, with the latter containing the antigen binding sites. For immunoPET applications, the use of small antibody fragment such as Fab, which exhibits rapid blood clearance, and positron emitters with suitable half-lives such as ^{64}Cu ($t_{1/2}$: 12.7 h) or ^{61}Cu ($t_{1/2}$: 3.4 h) can be advantageous.

The goal of this study was to investigate the in vitro and in vivo characteristics of ^{64}Cu-labeled TRC105-Fab for PET imaging of tumor angiogenesis in a 4T1 murine breast cancer model. Since radiolabeled Fab is expected to have rapid blood clearance and tumor uptake, we hypothesized that ^{61}Cu-labeling may also provide sufficient tumor contrast to allow visualization at early time points. The rationale for using ^{61}Cu as the PET isotope is that it has higher β^+ branching ratio (62% vs. 17%) and shorter decay half-life (3.4 h vs. 12.7 h) than ^{64}Cu, which is expected to provide a stronger PET signal and lower radiation dosimetry to normal organs than the corresponding ^{64}Cu-based PET tracer.

Materials and methods

Chemicals

TRC105 was provided by TRACON pharmaceuticals Inc. (San Diego, CA). AlexaFluor488- and Cy3-labeled secondary antibodies were purchased from Jackson Immunoresearch Laboratories, Inc. (West Grove, CA). *p*-SCN-Bn-NOTA (i.e. 2-S-(4-isothiocyanatobenzyl)-1,4,7-triazacyclononane-1,4,7-triacetic acid) was acquired from Macrocyclics, Inc. (Dallas, TX). Fluorescein isothiocyanate (FITC), hematoxylin staining solution, and Chelex 100 resin (50–100 mesh) were purchased from Sigma-Aldrich (St. Louis, MO). AlexaFluor350-NHS ester (NHS denotes N-hydroxysuccinimide) was acquired from Invitrogen (Grand Island, NY). Water and all buffers were of Millipore grade and pre-treated with Chelex 100 resin to ensure that the aqueous solution was heavy metal-free. PD-10 columns were purchased from GE Healthcare (Piscataway, NJ). Pierce immobilized papain (cat# 20341), Dionex ProPac WCX-10 weak cation-exchange column (4 × 250 mm), and all other reaction buffers and chemicals were purchased from Thermo Fisher Scientific (Fair Lawn, NJ).

Generation and characterization of TRC105-Fab

The digestion of TRC105 (2 mg/mL) was carried out in a reaction buffer (20 mM sodium phosphate monobasic, 10 mM disodium ethylenediaminetetraacetic acid [EDTA], and 80 mM cysteine.HCl) for 4 h at 37 °C, with immobilized papain:TRC105 weight ratio of 1:40 [16]. Afterwards, the reaction mixture was centrifuged at 5000×*g* for 1 min to remove the immobilized papain. The supernatant was purified with Sephadex G-75 size exclusion column chromatography to yield TRC105-Fab, using phosphate-buffered saline (PBS) as the mobile phase. The concentration of TRC105-Fab was determined from UV absorbance at 280 nm using an extinction coefficient of 1.4 mL/mg/cm [26].

The purity of TRC105-Fab was evaluated with sodium dodecyl sulfate polyacrylamide gel electrophoresis (SDS-PAGE; 5% stacking gel and 8% resolving gel; non-reducing conditions) using Coomassie brilliant blue R-250 staining. The molecular weight of TRC105-Fab was determined by matrix-assisted laser desorption/ionization (MALDI) mass spectrometry, which served as a reference for the TRC105-Fab band in SDS-PAGE. In addition, high performance liquid chromatography (HPLC) analysis was conducted to evaluate the purity of TRC105-Fab and TRC105 in a Dionex Ultimate 3000 system using the ProPac WCX-10 column. Eluent A: 20 mM 2-(*N*-morpholino)ethanesulfonic acid (MES), 1 mM EDTA, 40 mM NaCl, pH 5.5; Eluent B: 20 mM MES, 1 mM EDTA, 250 mM NaCl, pH 5.5. The NaCl gradient used was 3.75 mM/min with a flow rate of 1 mL/min. Absorbance at 280 nm was used for protein detection.

NOTA/FITC/AlexaFluor350 conjugation of TRC105-Fab and $^{61/64}$Cu-labeling

NOTA conjugation was carried out at pH 9.0, with the reaction ratio of *p*-SCN-Bn-NOTA:TRC105-Fab being 10:1. NOTA-TRC105-Fab was purified using PD-10 columns with PBS as the mobile phase. A similar reaction and purification procedure was adopted for conjugation of FITC (for flow cytometry analysis) or AlexaFluor350 NHS ester (for histology applications) onto TRC105-Fab, except that the reaction ratio of FITC or AlexaFluor350 NHS ester:TRC105-Fab was 3:1 to limit the number of dyes per TRC105-Fab and avoid self-quenching of the fluorescence signal.

The two PET isotopes were produced using ^{64}Ni(p,n)^{64}Cu and ^{60}Ni(d,n)^{61}Cu reactions, respectively. $^{64}CuCl_2$ or $^{61}CuCl_2$ (74 MBq) was diluted in 300 μL of 0.1 M sodium acetate buffer (pH 6.5) and added to 40 μg of NOTA-TRC105-Fab. The reaction mixture was incubated for 30 min at 37 °C with constant shaking, and $^{61/64}$Cu-NOTA-TRC105-Fab was

purified using PD-10 columns with PBS as the mobile phase. The radioactive fractions containing $^{61/64}$Cu-NOTA-TRC105-Fab were collected and passed through a 0.2 μm syringe filter before in vivo studies.

Flow cytometry

The CD105 binding affinity/specificity of TRC105-Fab was evaluated with fluorescence-activated cell sorting (FACS) analysis in two cell lines: human umbilical vein endothelial cells (HUVECs, high CD105 expression [13, 27]) and MCF-7 human breast cancer cells (CD105-negative [13, 28]). Cells were harvested and suspended in cold PBS (pH 7.4) with 2% bovine serum albumin at a concentration of 5×10^6 cells/mL, which were incubated with various concentrations of FITC-TRC105-Fab (5, 25, or 100 nM) for 30 min at room temperature, washed and centrifuged at 1,000 rpm for 5 min. Afterwards, the cells were analyzed by FACS using a BD FACSCalibur 4-color analysis cytometer (Becton-Dickinson, San Jose, CA) and FlowJo analysis software (Tree Star, Inc., Ashland, OR).

PET imaging and biodistribution studies

The 4T1 murine breast cancer model was generated as previously described [13, 29]. PET and PET/CT scans of tumor-bearing female BALB/c mice (6–8 weeks old, tumor diameter 5–8 mm) were performed using an Inveon microPET/microCT rodent model scanner (Siemens Medical Solutions USA, Inc.). Each mouse was intravenously injected with 5–10 MBq of $^{61/64}$Cu-NOTA-TRC105-Fab and 5 or 10 minute static PET scans were performed at various time points post-injection (p.i.). The images were reconstructed using a maximum a posteriori (MAP) algorithm, with no attenuation or scatter correction. Region-of-interest (ROI) analysis of each PET scan was performed using vendor software (Inveon Research Workplace [IRW]) on decay-corrected whole-body images as described previously [30, 31], to calculate the percentage injected dose per gram of tissue (%ID/g) values for the 4T1 tumor and several major organs.

Blocking studies were carried out to evaluate CD105 specificity of ^{64}Cu-NOTA-TRC105-Fab in vivo, where a group of 4 mice was each injected with 2 mg of TRC105 within 1 h before ^{64}Cu-NOTA-TRC105-Fab administration. After the last PET scans at 24 h p.i., mice were euthanized and the blood, 4T1 tumor, and major organs/tissues were collected and wet-weighed. The radioactivity in the tissue was measured using a Cobra II gamma-counter (Perkin-Elmer) and presented as %ID/g. The 4T1 tumor, liver, kidney (i.e. tissues with significant uptake of $^{61/64}$Cu-NOTA-TRC105-Fab), and muscle were also frozen and sectioned for histological analysis.

Histology

Frozen tissue slices of 7 μm thickness were fixed with cold acetone for 10 min and dried in the air for 30 min. After rinsing with PBS and blocking with 10% donkey serum for 30 min at room temperature, the slices were incubated with TRC105 (2 μg/mL) for 1 h at 4 °C and visualized using AlexaFluor488-labeled goat anti-human IgG. After washing with PBS, the tissue slices were also stained for endothelial marker CD31 as described previously [13]. Subsequently, the slices were incubated with AlexaFluor350-TRC105-Fab (2 μg/mL) for 30 min. Hematoxylin staining was also carried out to demarcate the cell nuclei in the tissue slices. After washing with PBS, all images were acquired with a Nikon Eclipse Ti microscope.

Statistical analysis

Quantitative data were presented as mean ± SD. Means were compared using Mann-Whitney U-test. P values < 0.05 were considered statistically significant.

Results

Generation and characterization of TRC105-Fab

Following papain digestion, TRC105-Fab was separated from other components in the reaction mixture using Sephadex G-75 column (fractionation range: 3,000–70,000 Da). The elution profile is shown in Fig. 1a and only the single fraction with the highest TRC105-Fab concentration was used for further studies (indicated by arrowhead). SDS-PAGE indicated disappearance of the TRC105 band expected at ~148 kDa and the appearance of pure TRC105-Fab (Fig. 1b), which was confirmed by HPLC analysis (Fig. 1c). Taken together, these findings indicated complete digestion of TRC105 after papain treatment to yield high purity TRC105-Fab for further bioconjugation and investigation. Mass spectrometry indicated that TRC105 has a molecular weight of ~148 kDa and TRC105-Fab has a molecular weight of ~47.5 kDa (Fig. 1d), which was consistent with the molecular weight predicted by amino acid analysis.

Flow cytometry analysis

As indicated in Fig. 2, treatment with FITC-TRC105-Fab significantly enhanced the mean fluorescence intensity of HUVECs (~12 fold higher than the unstained cells at 25 nM), whereas treatment with a “blocking” dose of TRC105 (1 μM) reduced the cell fluorescence by ~10 fold. These data demonstrated that FITC-TRC105-Fab specifically binds to CD105 on the HUVECs. Meanwhile, fluorescence signal on CD105-negative MCF-7 cells was minimal for all groups even when treated with FITC-TRC105-Fab at a much higher concentration (100 nM), indicating low non-specific binding of FITC-TRC105-Fab in cell culture. Overall, FACS studies demonstrated that FITC-TRC105-Fab exhibited strong and specific binding to CD105 on cells with minimal non-specific binding, indicating that papain digestion did not compromise the CD105 binding affinity/specificity of TRC105-Fab.

PET imaging and biodistribution studies

NOTA was chosen as the chelator in this study, since many literature reports have shown that it is one of the best chelators for ^{64}Cu-labeling [32–34]. $^{61/64}$Cu-labeling, including purification using PD-10 columns, took 60 ± 10 min (n = 8). The decay-corrected radiochemical yield was 50.2 ± 10.4%, based on 20 μg of NOTA-TRC105-Fab per 37 MBq of ^{64}Cu, with radiochemical purity of >95%. The specific activity was ~44 GBq/μmol, assuming complete recovery of NOTA-TRC105-Fab after size exclusion column chromatography.

The coronal PET slices that encompassed 4T1 tumors are shown in Fig. 3a and representative PET/CT fused images of a mouse at 5 h p.i. of ^{64}Cu-NOTA-TRC105-Fab is shown in Fig. 3b. ^{61}Cu-NOTA-TRC105-Fab exhibited similar in vivo distribution pattern as ^{64}Cu-NOTA-TRC105-Fab at early time points (Fig. 3c). Quantitative data obtained from ROI analysis of the PET results are shown in Fig. 4.

Due to the much smaller size compared to the parent antibody TRC105 (47.5 kDa vs. 148 kDa), ^{64}Cu-NOTA-TRC105-Fab was cleared through both the hepatobiliary and renal pathways. The liver take of ^{64}Cu-NOTA-TRC105-Fab was 19.7 ± 1.6, 18.0 ± 0.8, 12.8 ± 0.6, 8.3 ± 0.8, and 9.2 ± 0.4 %ID/g at 0.5, 2, 5, 16, and 24 h p.i. respectively (n = 4; Fig. 4a). Radioactivity in the blood was 8.7 ± 0.6, 7.3 ± 0.2, 4.7 ± 0.2, 3.5 ± 1.3, and 3.8 ± 0.2 %ID/g at 0.5, 2, 5, 16, and 24 h p.i. respectively (n = 4; Fig. 4a), indicating significantly faster clearance from the blood than ^{64}Cu-NOTA-TRC105, which had blood radioactivity level of 16.2 ± 1.9, 10.7 ± 2.0, and 8.3 ± 0.9 %ID/g at 4, 24, and 48 h p.i. respectively (n = 3) [34]. Importantly, tumor uptake of ^{64}Cu-NOTA-TRC105-Fab accumulated rapidly and was clearly visible as early as 0.5 h p.i., peaked at 5 h p.i., and remained prominent over time

(3.6 ± 0.4, 4.2 ± 0.5, 4.9 ± 0.3, 4.4 ± 0.7, and 4.6 ± 0.8 %ID/g at 0.5, 2, 5, 16, and 24 h p.i. respectively; n = 4; Fig. 3a, 4a). Because of the rapid blood clearance and tumor uptake of radiolabeled TRC105-Fab, ^{61}Cu-NOTA-TRC105-Fab was also able to provide tumor contrast at the time points of 3 and 8 h p.i. (Fig. 3c).

Administering a blocking dose of TRC105 significantly reduced the tumor uptake of ^{64}Cu-NOTA-TRC105-Fab to 1.8 ± 0.4, 2.3 ± 0.4, 2.6 ± 0.2, 2.9 ± 0.4, and 3.2 ± 0.4 %ID/g at 0.5, 2, 5, 16, and 24 h p.i. respectively (n = 4; $P < 0.05$ before 24 h p.i.; Fig. 3a, 4b,c), which demonstrated that ^{64}Cu-NOTA-TRC105-Fab maintained CD105 specificity in vivo. Liver uptake of ^{64}Cu-NOTA-TRC105-Fab in the blocking group was similar to mice injected with ^{64}Cu-NOTA-TRC105-Fab alone, however the kidney uptake was significantly lower at all time points examined (19.6 ± 3.6, 22.8 ± 4.3, 19.4 ± 5.2, 16.6 ± 3.2, and 13.6 ± 2.3 %ID/g at 0.5, 2, 5, 16, and 24 h p.i. respectively vs. 38.5 ± 5.6, 34.8 ± 4.2, 31.4 ± 5.0, 21.6 ± 2.2, and 20.5 ± 2.2 %ID/g at 0.5, 2, 5, 16, and 24 h p.i. respectively for mice injected with ^{64}Cu-NOTA-TRC105-Fab alone; n = 4; Fig. 4a,b).

Fig. 4c summarizes the 4T1 tumor uptake of the tracer for both groups. The differences in tumor %ID/g values were statistically significant ($P < 0.05$; n = 4) at all time points examined except 24 h p.i., when most of the tracer has already been cleared by the mice. After the last PET scans at 24 h p.i., biodistribution studies confirmed that the quantitation of tracer uptake based on PET imaging accurately reflected radioactivity distribution in tumor-bearing mice, as similar %ID/g values were calculated from PET and biodistribution results (Fig. 5). More importantly, the 4T1 tumor uptake of ^{64}Cu-NOTA-TRC105-Fab was higher than all major organs except the liver and kidneys (which are responsible for tracer clearance), thus providing good tumor contrast.

The peak uptake in the 4T1 tumor was lower for ^{64}Cu-NOTA-TRC105-Fab (4.9 ± 0.3 %ID/g at 5 h p.i.; n = 4) than ^{64}Cu-NOTA-TRC105 (13.0 ± 1.2 %ID/g at 48 h p.i.; n = 3), which is expected for radiolabeled antibody fragments [35]. However, the tumor-to-blood ratios were significantly better at early time points for ^{64}Cu-NOTA-TRC105-Fab (1.0 ± 0.2, 1.2 ± 0.2, and 1.2 ± 0.3 at 5, 16, and 24 h p.i. respectively; n = 4) than ^{64}Cu-NOTA-TRC105 (0.5 ± 0.1 and 1.0 ± 0.2 at 4 and 24 h p.i. respectively; n = 3), which is desirable for future clinical translation to allow for same day PET imaging following tracer injection. In addition, the possible use of ^{61}Cu instead of ^{64}Cu may increase the PET signal intensity (due to higher β^+ branching ratio) and reduce the radiation dosimetry to normal organs (attributed to shorter decay half-life).

Histology

Immunofluorescence CD105/CD31 co-staining of various tissues revealed that CD105 expression in the 4T1 tumor was primarily on the tumor vasculature, as evidenced by excellent co-localization of CD105 and CD31 staining and virtually undetectable signal on the 4T1 tumor cells (Fig. 6). The staining with AlexaFluor350-TRC105-Fab gave excellent overlay with both CD105 and CD31 staining in the 4T1 tumor, which confirmed that TRC105-Fab and $^{61/64}$Cu-NOTA-TRC105-Fab bind with good affinity and specificity to CD105 on the tumor vasculature.

CD105 staining of mouse liver and muscle gave very low intensity signals, indicating that these tissues do not have significant CD105 expression. Thus, uptake of $^{61/64}$Cu-NOTA-TRC105-Fab in the liver was largely attributed to non-specific hepatic clearance instead of CD105 mediated binding. The appreciable CD105 expression in the kidneys may be partially responsible for high tracer uptake in the kidneys, in addition to that attributed to renal clearance. This phenomenon may also explain the significantly lower tracer uptake in

the kidneys after a pre-injected blocking dose of TRC105, as part of ^{64}Cu-NOTA-TRC105-Fab uptake in the kidneys is CD105 specific.

Discussion

Tumor cells rely on the formation of new blood vessels for adequate nutrition during tumor growth. Tremendous effort has been devoted over the last two decades to discover specific markers for newly formed tumor vessels and a number of targets have been investigated for non-invasive imaging of tumor angiogenesis [2–4]. CD105 has several advantages over the other targets, including high-level expression in a wide variety of solid malignancies, independence from its expression on neoplastic cells (including the 4T1 tumor model employed here), lack of tumor histotype specificity, and immediate accessibility of malignant lesions through the blood stream [12, 36]. Our group has previously demonstrated the capability of various radiolabeled TRC105 for the non-invasive PET imaging of CD105 expression during tumor angiogenesis in several preclinical tumor models [13, 27, 29, 31, 34, 37].

Delayed tracer uptake in the tumor tissue and slow clearance from the circulation are two major hurdles faced by immunoPET with radiolabeled intact antibodies, which could be improved through the use of antibody fragments [15]. For imaging applications, achieving tumor contrast faster is highly desirable [38–40]. Therefore, the use of Fab or other engineered antibody fragments instead of intact antibodies as the targeting ligands can be advantageous [16–25]. Furthermore, intact antibodies may trigger immune responses that are not desirable for imaging applications.

TRC105 is a chimeric IgG1 monoclonal antibody composed of four peptide chains (two heavy and two light chains), with a molecular weight of ~148 kDa. Being a much smaller molecule of ~47.5 kDa, TRC105-Fab is expected to have a faster clearance from blood and an improved penetration into solid tumors. The caveat for using antibody fragment such as Fab is the lower tumor uptake of the tracer than the similarly labeled intact antibody, which was observed in this study. This phenomenon may be partially attributed to the decreased internalization efficiency of a Fab fragment because of the lack of Fc, which can play an important role in antibody internalization. On the other hands, the lack of Fc can eliminate non-specific binding between Fc and its receptors on various types of cells (e.g. macrophages, dendritic cells, neutrophils, natural killer cells, B cells etc.) and improve the tumor-to-normal tissue ratio [41]. The decreased uptake of ^{64}Cu-NOTA-TRC105-Fab in the mouse spleen compared to ^{64}Cu-NOTA-TRC105 may be partially attributed to the lack of Fc mediated binding. The uptake of ^{64}Cu-NOTA-TRC105-Fab in mouse kidneys may be unique to mouse tissue as antibodies to human CD105 have been reported to bind specifically to kidney tumors but not normal renal parenchyma [42].

The much faster blood clearance of ^{64}Cu-NOTA-TRC105-Fab compared to ^{64}Cu-NOTA-TRC105 enabled us to use the much shorter-lived ^{61}Cu as the radiolabel. ^{64}Cu can be used for both diagnostic and therapeutic applications while ^{61}Cu is primarily a diagnostic isotope. One major advantage of ^{61}Cu is that it yields better tomographic images than ^{64}Cu, due to higher β^+ branching ratio [43]. Furthermore, the use of ^{61}Cu instead of ^{64}Cu can not only decrease the radiation exposure to normal tissues of the body, but also reduce the cost for isotope production through the use of a deuteron beam for ^{61}Cu generation (^{60}Ni is significantly less expensive than ^{64}Ni, which is typically used to produce ^{64}Cu with a proton beam). Therefore, ^{61}Cu may be preferred over the more widely available ^{64}Cu for immunoPET with small antibody fragments. Several other PET isotopes also exhibit desirable characteristics for antibody fragment-based imaging (e.g. ^{45}Ti and ^{44}Sc, both have

similar half-lives as ^{61}Cu, high β^+ branching ratio, and low β^+ energy), which warrant future evaluation.

4T1 breast cancer is a highly vascularized tumor model that grows rapidly upon implantation and provides a sufficient number of vessels for in vivo imaging of angiogenesis (MVD of the 4T1 tumor was 205 ± 29 vessels/mm^2 based on CD105 histology; n = 8). In addition, CD105 targeted anti-angiogenic therapy has been shown to be effective in this tumor model [44]. One limitation of this model is that the tumor vasculature is of murine origin. TRC105 is known to have a significantly higher affinity to human CD105 than its murine homolog [45]. Therefore, it is possible that the tracer may perform better in future clinical applications than what was observed in experimental animal tumor models. With demonstrated affinity/specificity for CD105 in this study, radiolabeled TRC105-Fab has the potential to serve as promising imaging/diagnostic agents for same day immunoPET imaging in cancer patients in the future.

Conclusion

Herein we report the development, characterization, and in vivo investigation of a $^{61/64}$Cu-labeled Fab fragment of TRC105 for PET imaging of tumor angiogenesis in a murine breast cancer model. Rapid, prominent, and target specific uptake in the 4T1 tumor was observed for $^{61/64}$Cu-NOTA-TRC105-Fab. Further optimization and clinical translation of radiolabeled TRC105-Fab for PET imaging of tumor angiogenesis may play multiple roles in improving the management of cancer patients (e.g., patient stratification and treatment monitoring), as well as facilitate the development of novel anti-angiogenic drugs.

Acknowledgments

This work is supported, in part, by the University of Wisconsin Carbone Cancer Center, the Department of Defense (W81XWH-11-1-0644), and the Elsa U. Pardee Foundation.

References

1. Carmeliet P, Jain RK. Angiogenesis in cancer and other diseases. Nature. 2000; 407:249–257. [PubMed: 11001068]
2. Backer MV, Backer JM. Imaging key biomarkers of tumor angiogenesis. Theranostics. 2012; 2:502–515. [PubMed: 22737188]
3. Dijkgraaf I, Boerman OC. Radionuclide imaging of tumor angiogenesis. Cancer Biother Radiopharm. 2009; 24:637–647. [PubMed: 20025543]
4. Cai W, Chen X. Multimodality molecular imaging of tumor angiogenesis. J Nucl Med. 2008; 49(Suppl 2):113S–128S. [PubMed: 18523069]
5. Cai W, Rao J, Gambhir SS, Chen X. How molecular imaging is speeding up anti-angiogenic drug development. Mol Cancer Ther. 2006; 5:2624–2633. [PubMed: 17121909]
6. Backer MV, Levashova Z, Patel V, Jehning BT, Claffey K, Blankenberg FG, et al. Molecular imaging of VEGF receptors in angiogenic vasculature with single-chain VEGF-based probes. Nat Med. 2007; 13:504–509. [PubMed: 17351626]
7. Cai W, Niu G, Chen X. Imaging of integrins as biomarkers for tumor angiogenesis. Curr Pharm Des. 2008; 14:2943–2973. [PubMed: 18991712]
8. Zhang Y, Yang Y, Hong H, Cai W. Multimodality molecular imaging of CD105 (Endoglin) expression. Int J Clin Exp Med. 2011; 4:32–42. [PubMed: 21394284]
9. Cai W, Chen X. Multimodality imaging of vascular endothelial growth factor and vascular endothelial growth factor receptor expression. Front Biosci. 2007; 12:4267–4279. [PubMed: 17485373]
10. Wang RE, Niu Y, Wu H, Amin MN, Cai J. Development of NGR peptide-based agents for tumor imaging. Am J Nucl Med Mol Imaging. 2011; 1:36–46. [PubMed: 23133793]

11. Dallas NA, Samuel S, Xia L, Fan F, Gray MJ, Lim SJ, et al. Endoglin (CD105): a marker of tumor vasculature and potential target for therapy. Clin Cancer Res. 2008; 14:1931–1937. [PubMed: 18381930]
12. Fonsatti E, Nicolay HJ, Altomonte M, Covre A, Maio M. Targeting cancer vasculature via endoglin/CD105: a novel antibody-based diagnostic and therapeutic strategy in solid tumours. Cardiovasc Res. 2010; 86:12–19. [PubMed: 19812043]
13. Hong H, Yang Y, Zhang Y, Engle JW, Barnhart TE, Nickles RJ, et al. Positron emission tomography imaging of CD105 expression during tumor angiogenesis. Eur J Nucl Med Mol Imaging. 2011; 38:1335–1343. [PubMed: 21373764]
14. Rosen LS, Hurwitz HI, Wong MK, Goldman J, Mendelson DS, Figg WD, et al. A Phase I First-in-Human Study of TRC105 (Anti-Endoglin Antibody) in Patients with Advanced Cancer. Clin Cancer Res. 2012; 18:4820–4829. [PubMed: 22767667]
15. Wu AM, Olafsen T. Antibodies for molecular imaging of cancer. Cancer J. 2008; 14:191–197. [PubMed: 18536559]
16. Andrew SM, Pimm MV, Perkins AC, Baldwin RW. Comparative imaging and biodistribution studies with an anti-CEA monoclonal antibody and its $F(ab)_2$ and Fab fragments in mice with colon carcinoma xenografts. Eur J Nucl Med. 1986; 12:168–175. [PubMed: 3464424]
17. Hoeben BA, Kaanders JH, Franssen GM, Troost EG, Rijken PF, Oosterwijk E, et al. PET of hypoxia with ^{89}Zr-labeled cG250-$F(ab')_2$ in head and neck tumors. J Nucl Med. 2010; 51:1076–1083. [PubMed: 20554724]
18. Leyton JV, Olafsen T, Lepin EJ, Hahm S, Bauer KB, Reiter RE, et al. Humanized radioiodinated minibody for imaging of prostate stem cell antigen-expressing tumors. Clin Cancer Res. 2008; 14:7488–7496. [PubMed: 19010866]
19. Cai W, Olafsen T, Zhang X, Cao Q, Gambhir SS, Williams LE, et al. PET imaging of colorectal cancer in xenograft-bearing mice by use of an ^{18}F-labeled T84.66 anti-carcinoembryonic antigen diabody. J Nucl Med. 2007; 48:304–310. [PubMed: 17268029]
20. Olafsen T, Sirk SJ, Olma S, Shen CK, Wu AM. ImmunoPET using engineered antibody fragments: fluorine-18 labeled diabodies for same-day imaging. Tumour Biol. 2012; 33:669–677. [PubMed: 22392499]
21. Griffiths GL, Goldenberg DM, Roesch F, Hansen HJ. Radiolabeling of an anti-carcinoembryonic antigen antibody Fab' fragment (CEA-Scan) with the positron-emitting radionuclide Tc-94m. Clin Cancer Res. 1999; 5:3001s–3003s. [PubMed: 10541334]
22. Yoshida C, Tsuji AB, Sudo H, Sugyo A, Sogawa C, Inubushi M, et al. Development of positron emission tomography probe of ^{64}Cu-labeled anti-C-kit 12A8 Fab to measure protooncogene C-kit expression. Nucl Med Biol. 2011; 38:331–337. [PubMed: 21492781]
23. Burvenich IJ, Schoonooghe S, Blanckaert P, Bacher K, Vervoort L, Coene E, et al. Biodistribution and planar gamma camera imaging of ^{123}I- and ^{131}I-labeled $F(ab')_2$ and Fab fragments of monoclonal antibody 14C5 in nude mice bearing an A549 lung tumor. Nucl Med Biol. 2007; 34:257–265. [PubMed: 17383575]
24. Brouwers A, Mulders P, Oosterwijk E, Buijs W, Corstens F, Boerman O, et al. Pharmacokinetics and tumor targeting of ^{131}I-labeled $F(ab')_2$ fragments of the chimeric monoclonal antibody G250: preclinical and clinical pilot studies. Cancer Biother Radiopharm. 2004; 19:466–477. [PubMed: 15453961]
25. Sandstrom K, Haylock AK, Spiegelberg D, Qvarnstrom F, Wester K, Nestor M. A novel CD44v6 targeting antibody fragment with improved tumor-to-blood ratio. Int J Oncol. 2012; 40:1525–1532. [PubMed: 22307465]
26. Rousseaux J, Rousseaux-Prevost R, Bazin H. Optimal conditions for the preparation of Fab and $F(ab')_2$ fragments from monoclonal IgG of different rat IgG subclasses. J Immunol Methods. 1983; 64:141–146. [PubMed: 6644029]
27. Hong H, Severin GW, Yang Y, Engle JW, Zhang Y, Barnhart TE, et al. Positron emission tomography imaging of CD105 expression with ^{89}Zr-Df-TRC105. Eur J Nucl Med Mol Imaging. 2012; 39:138–148. [PubMed: 21909753]

28. Fonsatti E, Jekunen AP, Kairemo KJ, Coral S, Snellman M, Nicotra MR, et al. Endoglin is a suitable target for efficient imaging of solid tumors: *in vivo* evidence in a canine mammary carcinoma model. Clin Cancer Res. 2000; 6:2037–2043. [PubMed: 10815930]
29. Zhang Y, Hong H, Engle JW, Yang Y, Theuer CP, Barnhart TE, et al. Positron Emission Tomography and Optical Imaging of Tumor CD105 Expression with a Dual-Labeled Monoclonal Antibody. Mol Pharm. 2012; 9:645–653. [PubMed: 22292418]
30. Zhang Y, Hong H, Engle JW, Yang Y, Barnhart TE, Cai W. Positron emission tomography and near-infrared fluorescence imaging of vascular endothelial growth factor with dual-labeled bevacizumab. Am J Nucl Med Mol Imaging. 2012; 2:1–13. [PubMed: 22229128]
31. Zhang Y, Hong H, Severin GW, Engle JW, Yang Y, Goel S, et al. ImmunoPET and near-infrared fluorescence imaging of CD105 expression using a monoclonal antibody dual-labeled with ^{89}Zr and IRDye 800CW. Am J Transl Res. 2012; 4:333–346. [PubMed: 22937210]
32. Dearling JLJ, Voss SD, Dunning P, Snay E, Fahey F, Smith SV, et al. Imaging cancer using PET -- the effect of the bifunctional chelator on the biodistribution of a ^{64}Cu-labeled antibody. Nucl Med Biol. 2011; 38:29–38. [PubMed: 21220127]
33. Hong H, Benink HA, Zhang Y, Yang Y, Uyeda HT, Engle JW, et al. HaloTag: a novel reporter gene for positron emission tomography. Am J Transl Res. 2011; 3:392–403. [PubMed: 21904659]
34. Zhang Y, Hong H, Engle JW, Bean J, Yang Y, Leigh BR, et al. Positron emission tomography imaging of CD105 expression with a ^{64}Cu-labeled monoclonal antibody: NOTA is superior to DOTA. PLoS One. 2011; 6:e28005. [PubMed: 22174762]
35. Wu AM, Senter PD. Arming antibodies: prospects and challenges for immunoconjugates. Nat Biotechnol. 2005; 23:1137–1146. [PubMed: 16151407]
36. Seon BK, Haba A, Matsuno F, Takahashi N, Tsujie M, She X, et al. Endoglin-targeted cancer therapy. Curr Drug Deliv. 2011; 8:135–143. [PubMed: 21034418]
37. Hong H, Zhang Y, Severin GW, Yang Y, Engle JW, Niu G, et al. Multimodality Imaging of Breast Cancer Experimental Lung Metastasis with Bioluminescence and a Monoclonal Antibody Dual-Labeled with ^{89}Zr and IRDye 800CW. Mol Pharm. 2012; 9:2339–2349.
38. Grassi I, Nanni C, Allegri V, Morigi JJ, Montini GC, Castellucci P, et al. The clinical use of PET with ^{11}C-acetate. Am J Nucl Med Mol Imaging. 2012; 2:33–47. [PubMed: 23133801]
39. Vach W, Høilund-Carlsen PF, Fischer BM, Gerke O, Weber W. How to study optimal timing of PET/CT for monitoring of cancer treatment. Am J Nucl Med Mol Imaging. 2011; 1:54–62. [PubMed: 23133795]
40. Alauddin MM. Positron emission tomography (PET) imaging with ^{18}F-based radiotracers. Am J Nucl Med Mol Imaging. 2012; 2:55–76. [PubMed: 23133802]
41. Ravetch JV, Bolland S. IgG Fc receptors. Annu Rev Immunol. 2001; 19:275–290. [PubMed: 11244038]
42. Costello B, Li C, Duff S, Butterworth D, Khan A, Perkins M, et al. Perfusion of ^{99m}Tc-labeled CD105 Mab into kidneys from patients with renal carcinoma suggests that CD105 is a promising vascular target. Int J Cancer. 2004; 109:436–441. [PubMed: 14961584]
43. Williams HA, Robinson S, Julyan P, Zweit J, Hastings D. A comparison of PET imaging characteristics of various copper radioisotopes. Eur J Nucl Med Mol Imaging. 2005; 32:1473–1480. [PubMed: 16258764]
44. Tsujie M, Uneda S, Tsai H, Seon BK. Effective anti-angiogenic therapy of established tumors in mice by naked anti-human endoglin (CD105) antibody: differences in growth rate and therapeutic response between tumors growing at different sites. Int J Oncol. 2006; 29:1087–1094. [PubMed: 17016638]
45. Matsuno F, Haruta Y, Kondo M, Tsai H, Barcos M, Seon BK. Induction of lasting complete regression of preformed distinct solid tumors by targeting the tumor vasculature using two new anti-endoglin monoclonal antibodies. Clin Cancer Res. 1999; 5:371–382. [PubMed: 10037187]

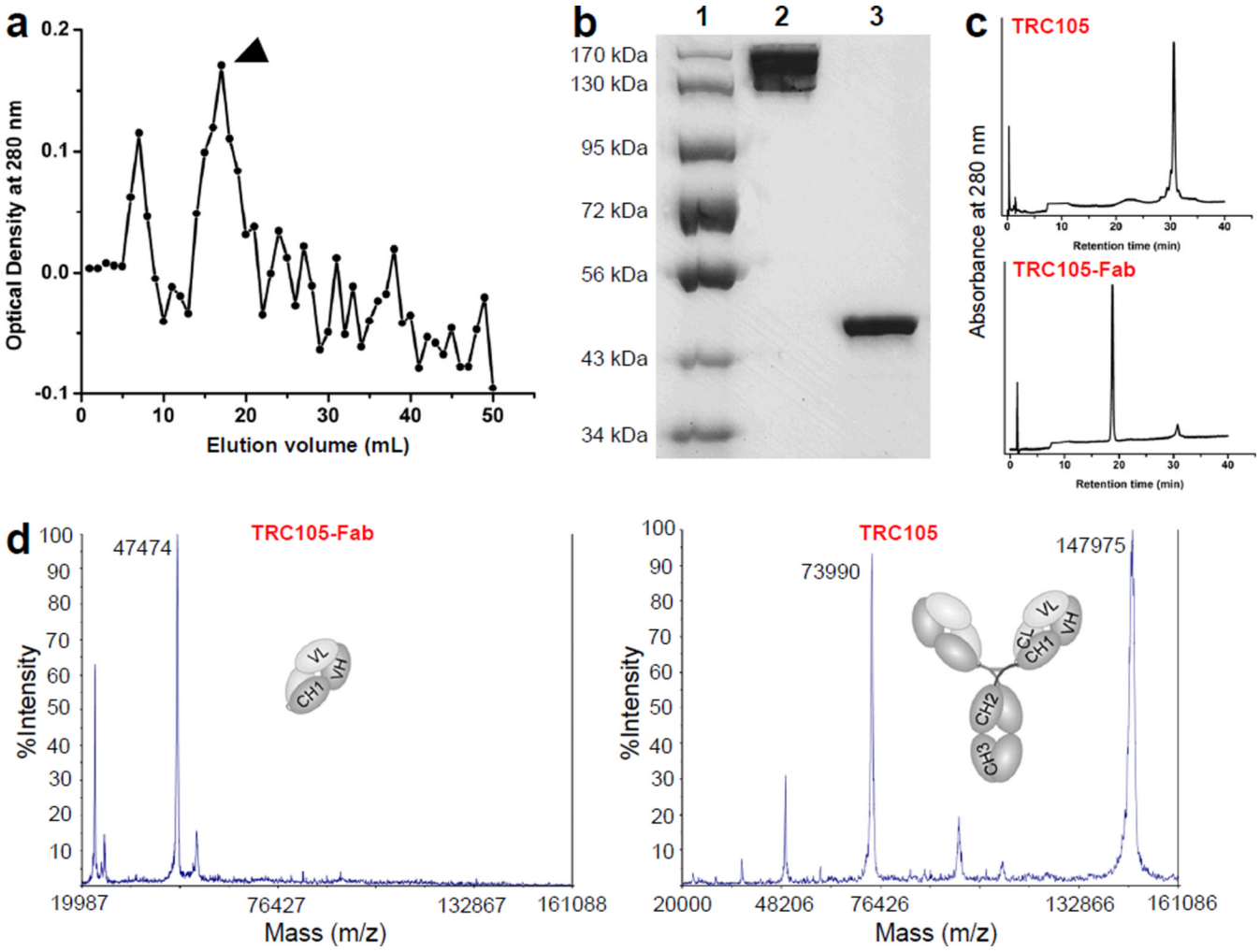

Fig. 1.

Purification and characterization of TRC105-Fab. **a** The elution profile of TRC105-Fab from a Sephadex G-75 column. Arrowhead indicates the single fraction used for further in vitro and in vivo studies. **b** SDS-PAGE confirmed the purity of TRC105-Fab. Lane 1: molecular weight markers; lane 2: TRC105; lane 3: TRC105-Fab after Sephadex G-75 column purification. **c** HPLC analysis of TRC105 and TRC105-Fab. **d** Mass spectrometry of TRC105-Fab (~47.5 kDa) and its parent antibody TRC105 (~148 kDa). Doubly charged ion is also observed for TRC105 in the mass spectrum (i.e., 73,990 Da).

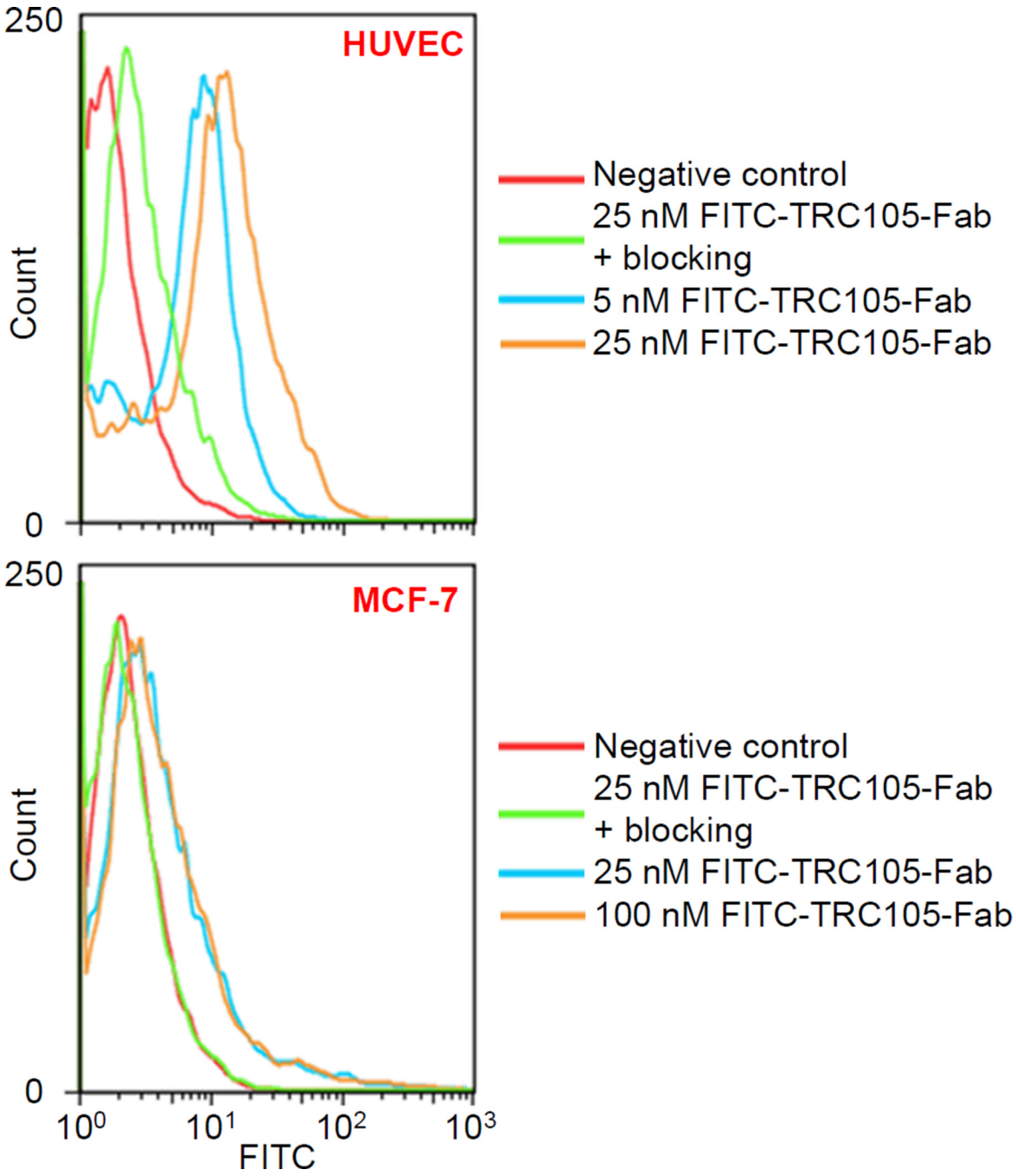

Fig. 2.
Flow cytometry analysis in CD105-positive HUVEC and CD105-negative MCF-7 cells confirms the CD105 specificity and affinity of TRC105-Fab.

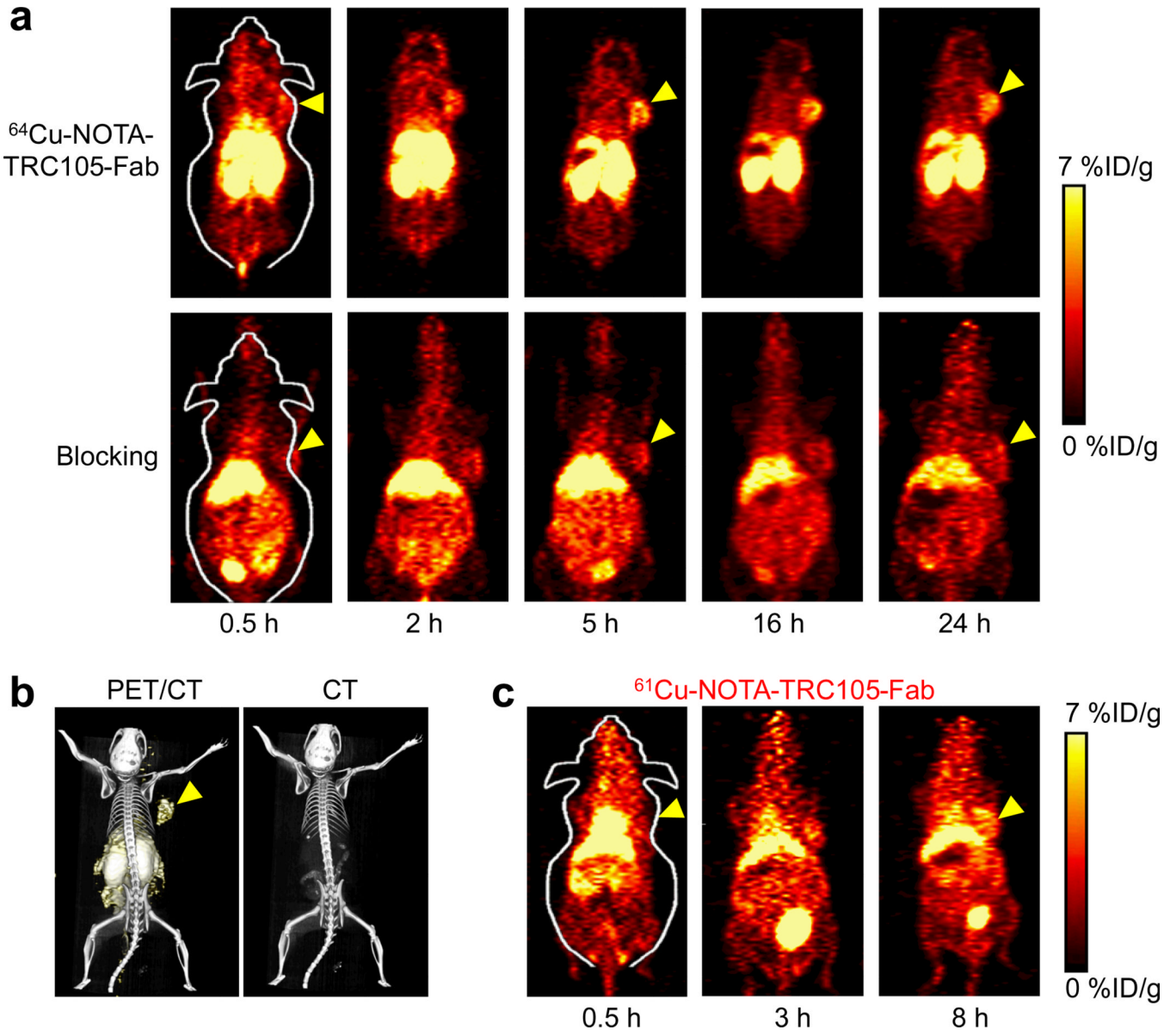

Fig. 3.

Serial PET imaging of CD105 expression in 4T1 tumor-bearing BALB/c mice. **a** Serial coronal PET images at 0.5, 2, 5, 16, and 24 h post-injection of ^{64}Cu-NOTA-TRC105-Fab, or ^{64}Cu-NOTA-TRC105-Fab after a pre-injected 2 mg blocking dose of TRC105. **b** Representative PET/CT images of 4T1 tumor-bearing mice at 5 h post-injection of ^{64}Cu-NOTA-TRC105-Fab. **c** Serial coronal PET images at 0.5, 3, and 8 h post-injection of ^{61}Cu-NOTA-TRC105-Fab in 4T1 tumor-bearing mice. Arrowheads indicate the 4T1 tumors.

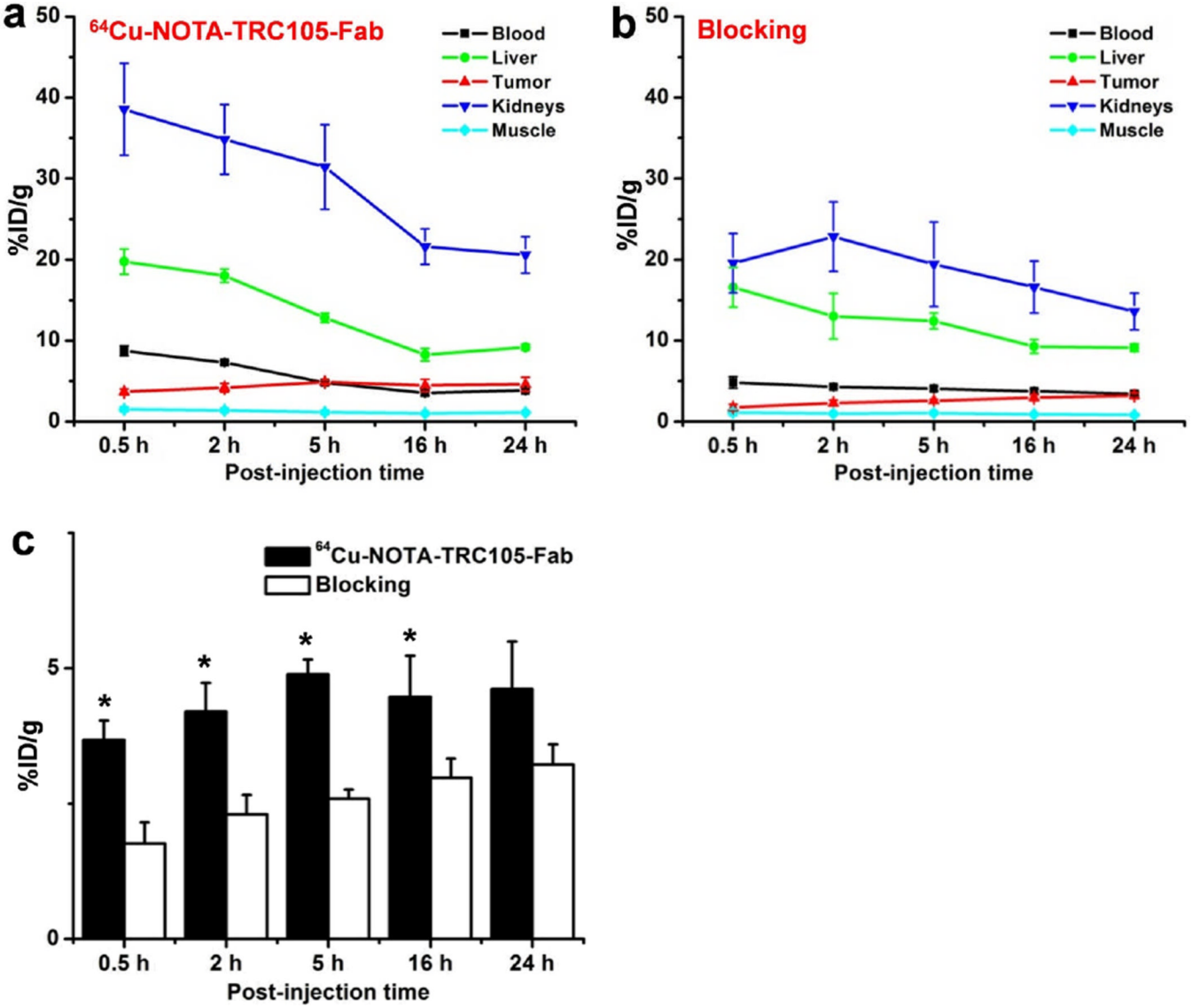

Fig. 4.

Quantitative analysis of the PET data. **a** Time-activity curves of the liver, 4T1 tumor, blood, kidney, and muscle upon intravenous injection of ^{64}Cu-NOTA-TRC105-Fab. **b** Time-activity curves of the liver, 4T1 tumor, blood, kidney, and muscle upon intravenous injection of ^{64}Cu-NOTA-TRC105-Fab, following a blocking dose of TRC105. **c** Comparison of tracer uptake in the 4T1 tumors between the two groups. $n = 4$; *, $P < 0.05$.

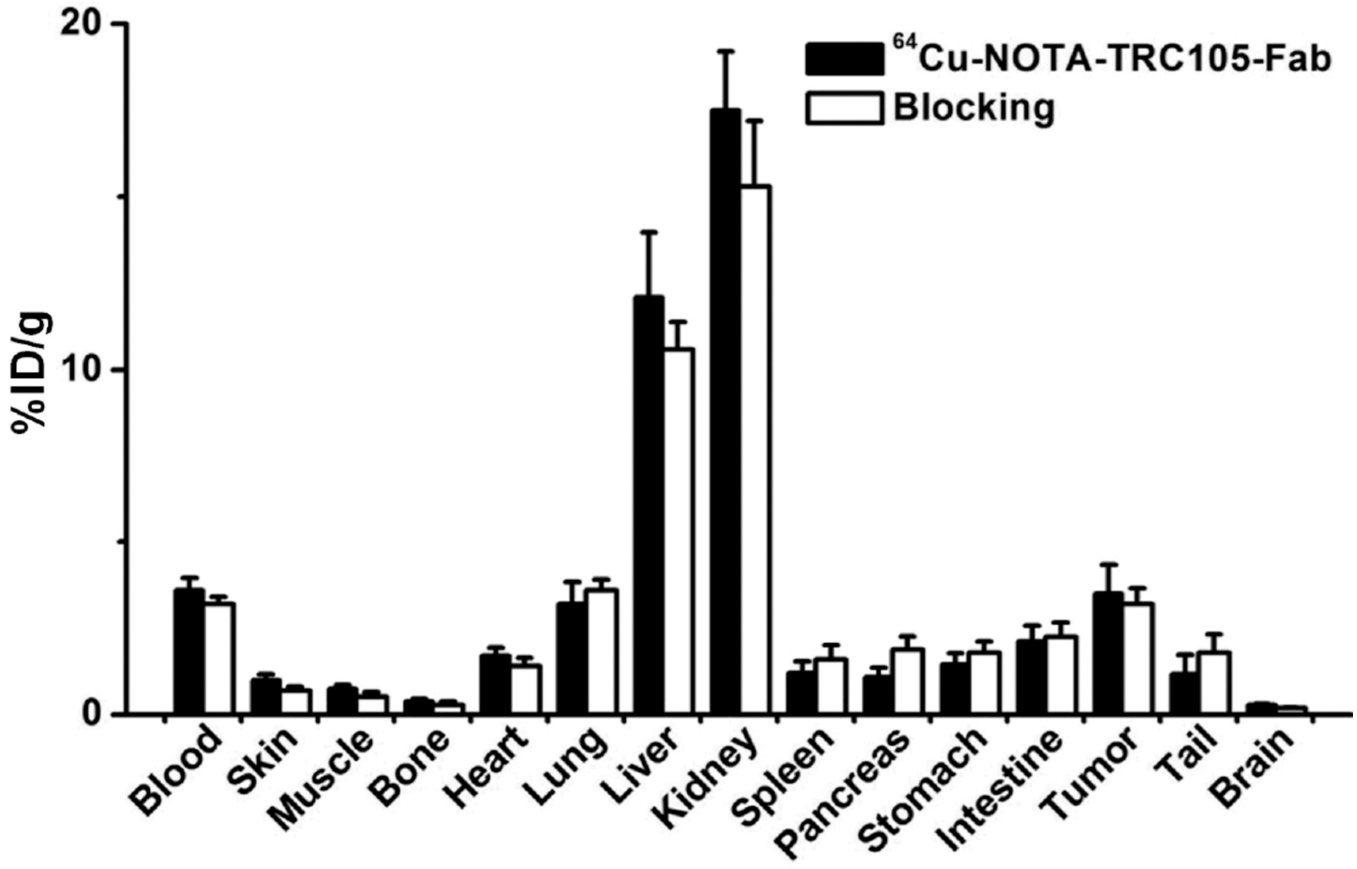

Fig. 5.
Biodistribution of ^{64}Cu-NOTA-TRC105-Fab, or ^{64}Cu-NOTA-TRC105-Fab after a blocking dose of TRC105, in 4T1 tumor-bearing mice at 24 h post-injection. n = 4.

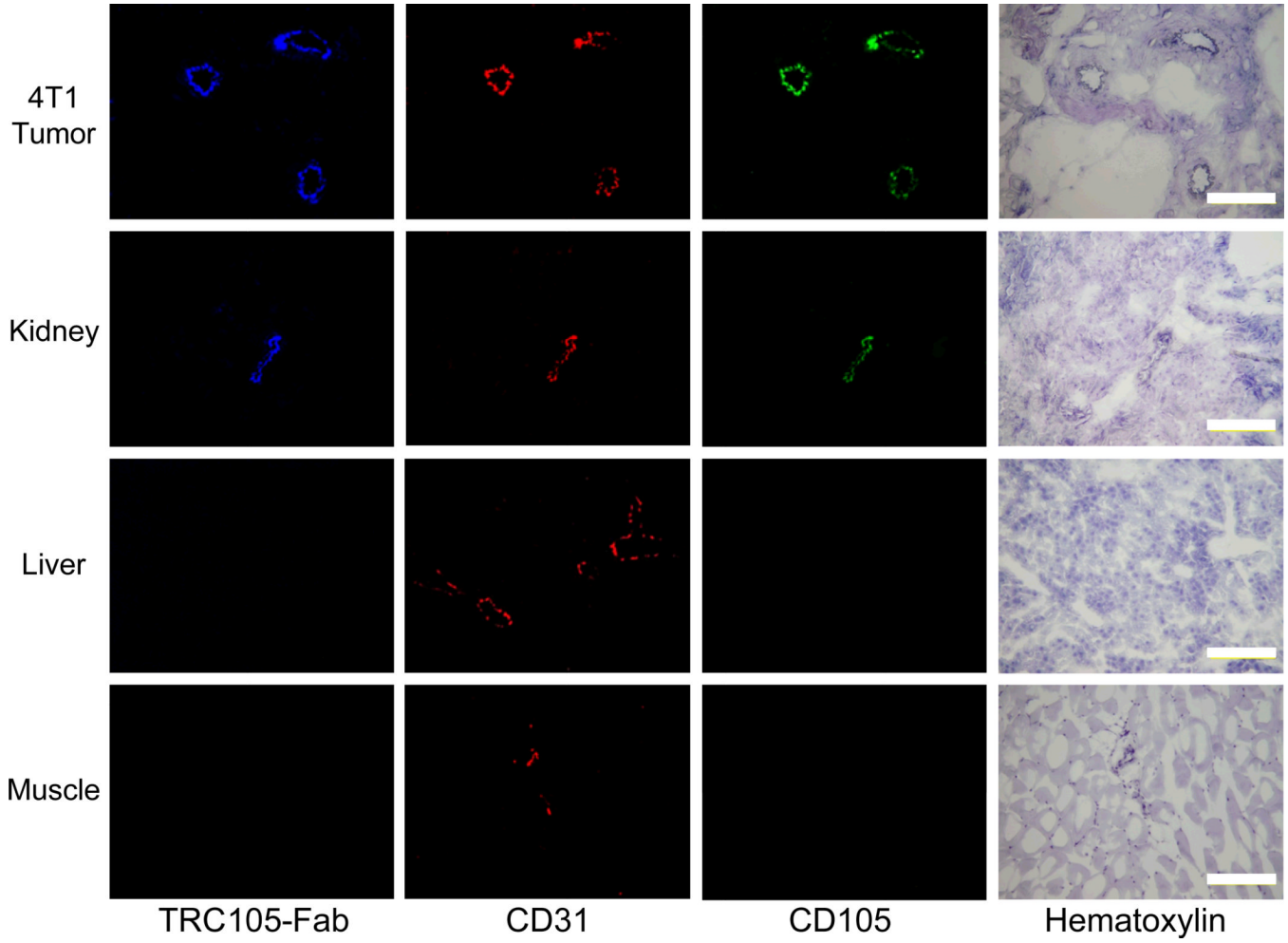

Fig. 6.

Immunofluorescence staining of 4T1 tumor, liver, kidney, and muscle tissue sections. TRC105 and AlexaFluor488-labeled goat anti-human IgG were used for CD105 staining (green). Rat anti-mouse CD31 antibody and Cy3-labeled donkey anti-rat IgG were used for CD31 staining (red). AlexaFluor350-TRC105-Fab (blue) was used to evaluate its overlay with CD105/CD31 staining. Hematoxylin staining was conducted to reveal the location of cell nuclei. Magnification: 200 ×. Scale bar: 50 μm.